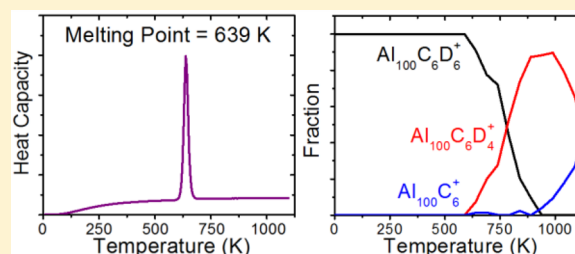


Dehydrogenation of Benzene on Liquid Al_{100}^+

Katheryne L. Leslie and Martin F. Jarrold*

Chemistry Department, Indiana University, 800 East Kirkwood Avenue, Bloomington, Indiana 47405, United States

ABSTRACT: The reactions of benzene on Al_{100}^+ have been investigated as a function of cluster temperature (300–1100 K) and relative kinetic energy (1–14 eV) by low-energy ion-beam methods and mass spectrometry. Benzene chemisorbs on both solid and liquid aluminum clusters to generate $\text{Al}_{100}\text{C}_6\text{D}_6^+$. A series of Al_{100-n}^+ ($n = 1, 2, 3, \dots$) products was also observed. As the cluster temperature was raised above the melting temperature of Al_{100}^+ , the $\text{Al}_{100}\text{C}_6\text{D}_6^+$ product dehydrogenates to form $\text{Al}_{100}\text{C}_6\text{D}_4^+$, $\text{Al}_{100}\text{C}_6\text{D}_2^+$, and $\text{Al}_{100}\text{C}_6^+$. The degree of dehydrogenation was measured as a function of temperature. Very little $\text{Al}_{100}\text{C}_6\text{D}_2^+$ was observed, suggesting that the losses of the second and third D_2 molecules are coordinated.



■ INTRODUCTION

Reactions on well-defined metal surfaces have been studied for many years. It is now well established that the surface structure influences the reactivity and that some low-index surfaces are a lot more reactive than others.^{1–6} Over the years, a lot of valuable information has been obtained from studying surface chemistry as a function of temperature.^{7–10} However, the temperatures employed rarely extend beyond the melting point of the surface, partly because most macroscopic metals melt at a very high temperature. As a consequence, not much is known about the reactivity of liquid metal surfaces and how the chemistry changes when the surface melts. The change in surface structure upon melting might be expected to cause a change in reactivity. In addition, the liquid can more easily adjust to accommodate a chemisorbed molecule, and products can more easily diffuse and dissolve in liquid metal.

It was first suggested more than a century ago that small particles have depressed melting temperatures because of the increase in the surface-to-volume ratio as the particle becomes smaller.¹¹ This melting-point depression, confirmed experimentally over 50 years ago,^{12–14} can be exploited to investigate the reactivity of liquid metal surfaces at temperatures that are well below the melting point of the macroscopic metal.

We have used this idea and investigated the role of phase in some reactions with aluminum clusters. These studies were performed with size-selected clusters, isolated in the gas phase, and they built on prior work where the melting temperatures were measured. It is only recently that methods have been developed to measure the melting temperatures for unsupported metal clusters with a precisely known number of atoms.^{15–20} These methods depend on measuring the heat capacity of size-selected clusters as a function of temperature. The melting transition is indicated by a peak in the heat capacity. Melting temperatures have been determined for a wide range of sizes for sodium and aluminum clusters.^{15–19,21–24}

In previous work, the reactions of Al_{100}^+ with N_2 and CO_2 were investigated as a function of cluster temperature and relative kinetic energy.^{25,26} Al_{100}^+ has a well-defined melting transition (with a relatively large latent heat) centered at around 639 K.²⁴ This is significantly below the bulk melting point of 934 K. The kinetic energy threshold for N_2 chemisorption on Al_{100}^+ was measured as a function of cluster temperature. Chemisorption of N_2 is an activated process on both liquid and solid Al_{100}^+ , but when the cluster melts, the threshold drops by around 1 eV, which corresponds to a 10^8 -fold increase in the reaction rate.²⁵ A combined experimental and theoretical study was performed on the analogous reaction with Al_{44}^{\pm} , which showed a similar decrease in the kinetic energy threshold when the cluster melted.²⁷ Density functional theory (DFT) was used to investigate the origin of the enhanced reactivity of the liquid cluster. The DFT studies suggested that the enhancement is a result of a volume change and an increase in atomic disorder when the cluster melts.²⁷ For the reaction between Al_{100}^+ and CO_2 , different products are generated depending on the phase of the cluster.²⁶ When the cluster is solid, only addition products are observed ($\text{Al}_{100}\text{CO}_2^+$ and $\text{Al}_{100}\text{O}^+$). When the cluster melts, secondary products are generated through the loss of neutral Al_2O from the addition products. The secondary products become more abundant as the temperature is raised above the melting temperature.

As reported in this article, we have investigated the reaction between benzene and Al_{100}^+ as a function of cluster temperature and relative kinetic energy. Benzene is a prototypic aromatic hydrocarbon, and so, there is a great deal of interest in its adsorption and dehydrogenation. The interactions between benzene and metals including gold, silver, and copper, to name but a few, have been the subjects of numerous theoretical and experimental studies.^{1,2,5,6,28–30} However, these studies have

Received: November 15, 2012

Revised: January 23, 2013

Published: February 28, 2013

focused on the interaction between benzene and the metal surfaces or individual metal atoms. Transition-metal surfaces including platinum, palladium, nickel, and niobium are known to dehydrogenate aromatic molecules.^{10,31,32} Size selectivity for benzene dehydrogenation has also been investigated for niobium clusters.³³

EXPERIMENTAL METHODS

The experimental apparatus and methods have been described in detail elsewhere.^{19,26} Briefly, a 99.999% aluminum target was resistively heated to above its melting point and ablated into a cooled helium buffer gas by a pulsed excimer laser. A liquid target was used because the resulting signal was much more stable than that obtained with a solid target.³⁴ The ablated metal atoms condensed to form clusters in the source region. The clusters were then carried by the buffer gas flow into a variable-temperature extension. The temperature of the extension was regulated to within ± 2 K by a microprocessor-based controller. The clusters undergo enough collisions with the buffer gas in the extension to be fully thermalized. The clusters exit the extension through a small aperture and were then focused into a quadrupole mass filter.

In the quadrupole, one cluster size was isolated by its mass-to-charge ratio. The size-selected clusters were then focused into a reaction cell where the reactant (deuterated benzene vapor) was introduced. C_6D_6 was used instead of C_6H_6 because deuterium is easier to resolve by mass spectrometry than hydrogen. The reaction cell was at room temperature. The pressure of the reactant in the reaction cell was kept at around 0.7 mTorr to minimize the number of secondary collisions. Reactant and product ions that passed through the collision cell were focused into a second quadrupole mass filter where they were analyzed. The kinetic energy of the ions exiting the collision cell depends on their mass. To avoid energy discrimination in the focusing of the ions into the quadrupole and in their transmission through the quadrupole, one of the voltages on the focusing lens and the quadrupole pole-offset voltage were scanned with the m/z ratio transmitted by the quadrupole.²⁶ SIMION simulations were performed to set up the scanning algorithms. After transmission through the second quadrupole, the ions were detected by an orthogonal collision dynode and dual microchannel plates (Photonis, Sturbridge, MA).

The kinetic energy of the cluster ions was set by the potential difference between the source and the collision cell. Mass spectra were measured as a function of both the relative kinetic energy and the temperature of the cluster ions. A Fortran program was used to subtract an average baseline from the measured spectra and integrate the peaks according to a user-defined list of peak boundaries. The peak areas were then used to calculate total reaction cross sections and cross sections for individual products. The following equation was used to calculate the total reaction cross section

$$\sigma_{\text{total}} = -\ln\left(\frac{I_{\text{R}}}{I_{\text{R}} + \sum I_{\text{P}}}\right)\left(\frac{1}{d}\right) \quad (1)$$

where I_{R} is the intensity of the remaining parent cluster and $\sum I_{\text{P}}$ is the sum of intensities of all products generated. The target density, d , is the product of the length of the reaction cell and the reagent number density. The cross sections for the individual products were obtained from the equation

$$\sigma_{\text{indiv}} = \sigma_{\text{total}}\left(\frac{I_{\text{indiv}}}{\sum I_{\text{P}}}\right) \quad (2)$$

where I_{indiv} is the intensity of the individual product.

RESULTS

Two types of experiments were performed in this study. In the first, we fixed the cluster temperature and measured reaction cross sections as a function of collision energy, whereas in the second, we fixed the collision energy and performed measurements as a function of the cluster temperature. The first type of experiments was performed at three temperatures: 573, 873, and 1073 K.

Figure 1 shows cross sections measured over a range of collision energies for the reaction between deuterated benzene

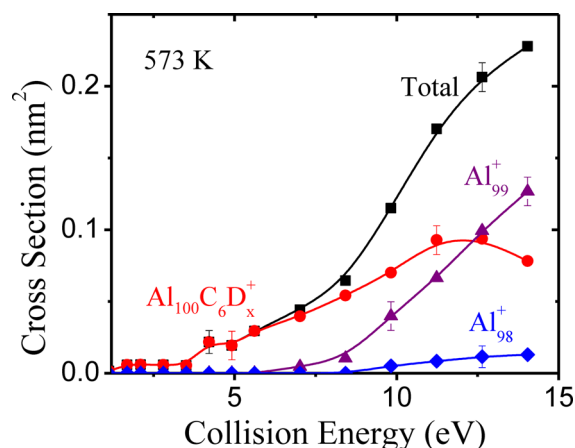


Figure 1. Plot of the total cross sections and the cross sections for the main single-collision products from the reaction of C_6D_6 with Al_{100}^+ at a cluster temperature of 573 K. Error bars show the estimated uncertainties.

and Al_{100}^+ at a temperature of 573 K. This temperature is 66 K below the melting temperature of the Al_{100}^+ cluster, which is 639 K.²⁴ Both the total cross sections and the cross sections for individual products are shown in Figure 1. At collision energies of less than 4 eV, the total cross section is very small (<0.01 nm²). There is a jump in the total cross section at around 4 eV due to the $Al_{100}C_6D_x^+$ product. This product results from the addition of a benzene molecule to the Al_{100}^+ cluster. We identify the product as $Al_{100}C_6D_x^+$ because, at higher temperatures, deuterated benzene is dehydrogenated. To separate the dehydrogenation products, the mass-resolving power must be increased to the point where the signal intensity is seriously impacted. Therefore, the bulk of the measurements reported here were performed with low mass-resolving power, and the dehydrogenation products were not resolved. Hence, we grouped them together as $Al_{100}C_6D_x^+$. A separate set of experiments using higher mass-resolving power to separate the dehydrogenation products is described later in this section.

As the collision energy was increased to around 6 eV, another product emerges: Al_{99}^+ . Above around 8 eV, the cross sections for Al_{99}^+ begin to increase rapidly, reaching around 0.13 nm² at the highest collision energy studied, where Al_{99}^+ is the most abundant product. A minor product, Al_{98}^+ , also emerges. It has a cross section of around 0.01 nm² at the highest collision energy studied.

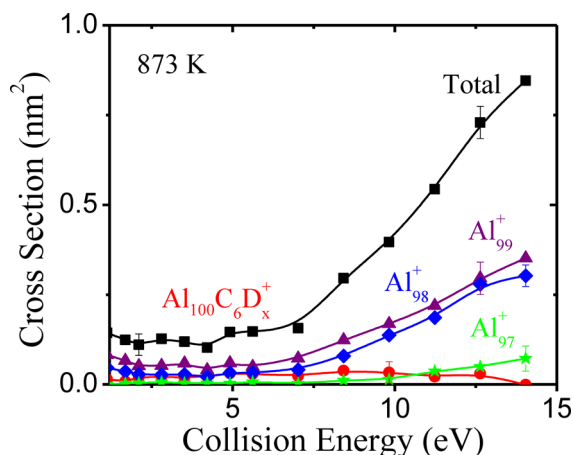
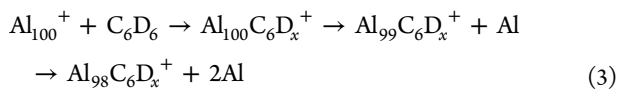


Figure 2. Plot of the total cross sections and the cross sections for the main single-collision products from the reaction of C_6D_6 with Al_{100}^+ at a cluster temperature of 873 K. Error bars show the estimated uncertainties.

Figure 2 shows data obtained at the second temperature, 873 K, which is 234 K above the melting temperature. At this temperature, the total reaction cross section is significantly above zero for all collision energies investigated. At low collision energies, the total cross section is fairly constant at around 0.15 nm^2 . Above 7 eV, the total cross section begins to increase nearly linearly, reaching a maximum of 0.85 nm^2 at the highest collision energy studied.

The cross sections for $Al_{100}C_6D_x^+$ increase slightly at the lower kinetic energies, level off at around 0.035 nm^2 , and then decrease at the higher kinetic energies. At the higher kinetic energies, the $Al_{100}C_6D_x^+$ cross sections are significantly smaller than those found at 573 K. Also, the jump in the $Al_{100}C_6D_x^+$ cross section that occurs at around 4 eV for a cluster temperature of 573 K is not present at 873 K. The cross sections simply show a gentle decrease with decreasing collision energy. Two related products, namely, $Al_{99}C_6D_x^+$ and $Al_{98}C_6D_x^+$, were also observed. These products were not found at the lower temperature. They were present only at low abundance at 873 K, so their cross sections are not shown in Figure 2. The cross sections for $Al_{99}C_6D_x^+$ and $Al_{98}C_6D_x^+$ show the same weak dependence on kinetic energy as found for $Al_{100}C_6D_x^+$. This observation rules out a mechanism whereby the $Al_{99}C_6D_x^+$ and $Al_{98}C_6D_x^+$ products are formed by sequential loss of aluminum atoms according to the scheme



A mechanism involving the sequential loss of aluminum atoms would be expected to lead to a significant shift in the kinetic energy thresholds as more aluminum atoms are lost.

The most abundant product found at 873 K is Al_{99}^+ . The cross sections for this product show the same general profile as the total cross section (see Figure 2) but with lower values. At low collision energies, the cross sections for Al_{99}^+ are roughly constant at around 0.05 nm^2 . Near 7 eV, the cross sections began to increase roughly linearly, to reach a maximum value of 0.3 nm^2 at the highest collision energy studied. Cross sections for Al_{98}^+ are similar to those for Al_{99}^+ . In addition to Al_{99}^+ and Al_{98}^+ , we also detected small amounts of Al_{97}^+ , Al_{96}^+ , Al_{95}^+ , and Al_{94}^+ . The cross sections for these products show the same

general behavior as found for Al_{99}^+ and Al_{98}^+ , except that the cross sections become smaller as the product ion becomes smaller. We show results for only the major products in Figure 2. However, all products were considered in calculating the total cross sections.

The cross sections measured at 1073 K, 434 K above the melting transition, are shown in Figure 3. The results at 1073 K

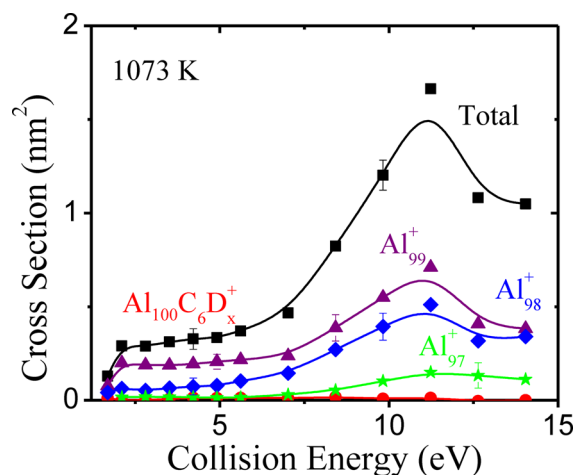


Figure 3. Plot of the total cross sections and the cross sections for the main single-collision products from the reaction of C_6D_6 with Al_{100}^+ at a cluster temperature of 1073 K. Error bars show the estimated uncertainties.

are similar to those at 873 K. Below a collision energy of 7 eV, the total cross section remain at around 0.3 nm^2 . Above 7 eV, the total cross sections increase rapidly, peaking at around 1.6 nm^2 near 11 eV and then falling as the collision energy is raised further. Comparing the results for all temperatures, it is evident that the magnitude of the total cross section systematically increases as the temperature is raised.

The dominant products found at 1073 K are similar to those found at 873 K and result from the loss of aluminum atoms to yield a series of Al_n^+ ions. Cross sections of Al_{99}^+ , Al_{98}^+ , and Al_{97}^+ are shown in Figure 3. As is evident from Figure 3, the cross sections for the Al_n^+ products decrease as the product ion becomes smaller. The cross sections for these products follow the profile of the total reaction cross section: constant at low collision energies, a relatively sharp linear increase starting at around 6–7 eV, a peak near 11 eV, and then a fall off at high collision energies.

A small amount of $Al_{100}C_6D_x^+$ was detected at 1073 K. The behavior of the cross sections for this product is similar to that of the corresponding cross sections at 873 K. They increase gently with increasing collision energy, plateau, and then fall off at higher collision energy. The plateau occurs at around 0.015 nm^2 , around half the value at 873 K.

For the second set of experiments, the collision energy was fixed at 7 eV, and the temperature was varied from 289 to 1039 K in increments of 50 K. The results of these experiments are shown in Figure 4, where cross sections are plotted against temperature.

At the lowest temperatures, the dominant product is $Al_{100}C_6D_x^+$. The cross section for $Al_{100}C_6D_x^+$ increase as the temperature is raised, peaks at around 600 K, and then decrease. The other major products observed in this set of experiments are Al_{99}^+ , Al_{98}^+ , and Al_{97}^+ . The cross sections for

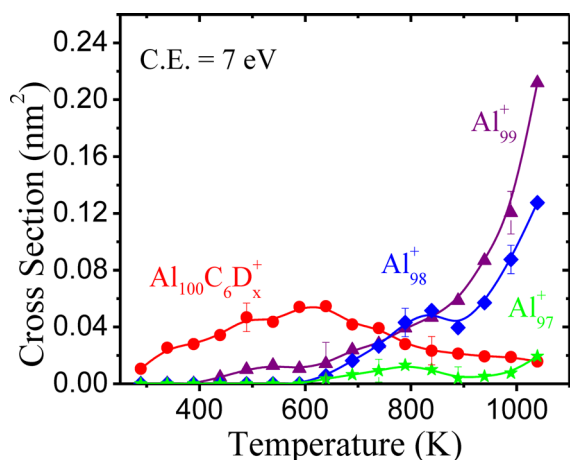


Figure 4. Plot of the cross sections measured for the main single-collision products from the reaction between C_6D_6 and Al_{100}^+ as a function of cluster temperature. The collision energy was 7 eV. Error bars show the estimated uncertainties.

Al_{98}^+ and Al_{97}^+ have a threshold at around 650 K. The cross sections for Al_{99}^+ also start to increase rapidly at 650 K, but in addition, Al_{99}^+ has a small tail that extends down to around 400 K. As before, some smaller Al_n^+ products were detected in low abundance, and they are not shown in Figure 4. The dips in the cross sections for Al_{98}^+ and Al_{97}^+ at the higher collision energies appear to be real features.

At high temperatures, the $Al_{100}C_6D_6^+$ species formed from a collision between an Al_{100}^+ cluster and a deuterated benzene molecule undergoes successive loss of D_2 molecules. The mass-resolving power used to perform the experiments described above was insufficient to separate the dehydrogenation products, so a separate set of experiments with a higher mass-resolving power was performed. Even with the higher resolution, we were not able to completely resolve the dehydrogenation products, so the measured mass spectra were fit using a Fortran program to deduce the relative amounts of the dehydrogenation products. We used the measured mass spectrum of the parent Al_{100}^+ ion shifted by the appropriate mass to fit the four peaks for $Al_{100}C_6D_6^+$, $Al_{100}C_6D_4^+$, $Al_{100}C_6D_2^+$, and $Al_{100}C_6^+$. The relative abundances of the four peaks were adjusted using a least-squares criterion to provide the best fit to the measured spectrum. An example is shown in Figure 5. The upper half of Figure 5 shows the peak measured for the $Al_{100}C_6D_x^+$ ions at 589 K. The black line represents the experimental data, and the green line is the fit. At 589 K, the only $Al_{100}C_6D_x^+$ species present is $Al_{100}C_6D_6^+$. The lower half of Figure 5 shows the mass spectrum measured at 789 K. At this temperature, around half of the $Al_{100}C_6D_6^+$ is dehydrogenated to give $Al_{100}C_6D_4^+$.

Figure 6 shows a plot of the relative abundances of the $Al_{100}C_6D_6^+$, $Al_{100}C_6D_4^+$, $Al_{100}C_6D_2^+$, and $Al_{100}C_6^+$ ions as a function of temperature, determined by fitting the $Al_{100}C_6D_x^+$ mass spectra. It is evident from these results that the dehydrogenation reaction turns on at around 600 K and, between 600 and 900 K, the amount of $Al_{100}C_6D_6^+$ decreases roughly linearly with temperature and $Al_{100}C_6D_4^+$ increases roughly linearly. Above 1000 K, $Al_{100}C_6D_4^+$ declines, and $Al_{100}C_6^+$ increases. Note that the amount of $Al_{100}C_6D_2^+$ remains small; therefore, the losses of the second and third D_2 molecules appear to be correlated.

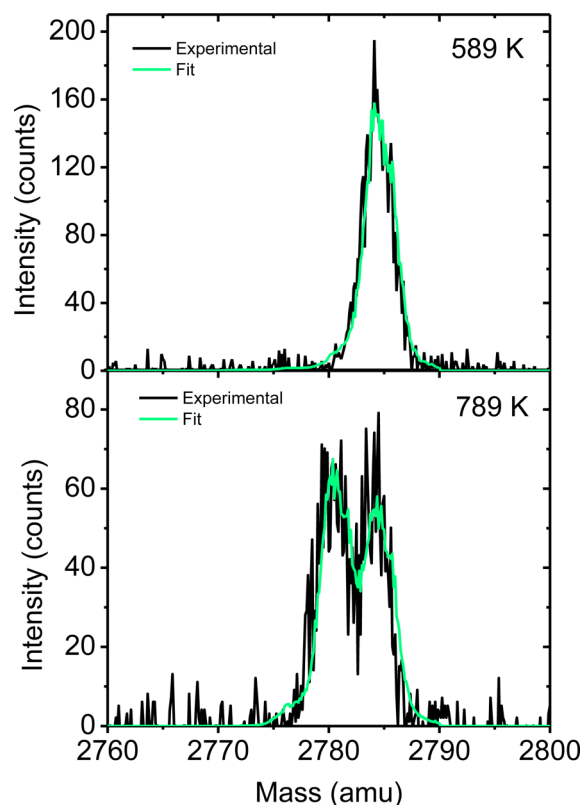


Figure 5. Experimental mass spectra (black) and calculated fits (green) of the $Al_{100}C_6D_x^+$ peak recorded below the melting point of Al_{100}^+ (589 K, top panel) and above the melting point (789 K, bottom panel). The collision energy was 7 eV.

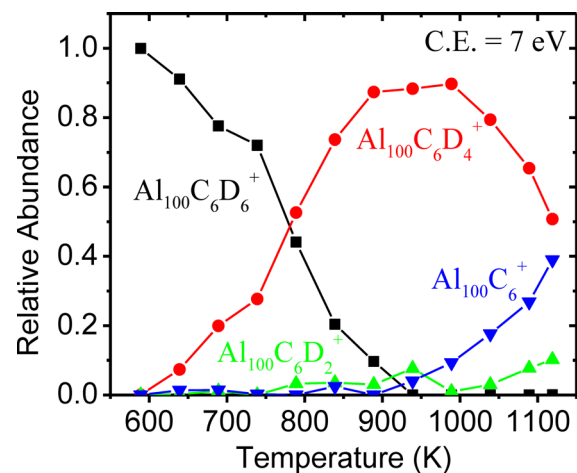
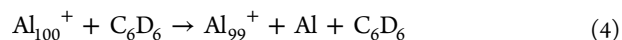


Figure 6. Plot of the relative abundances for each $Al_{100}C_6D_x^+$ product as a function of cluster temperature. The collision energy was 7 eV.

DISCUSSION

Two groups of products result from C_6D_6 collisions with Al_{100}^+ : $Al_{100}C_6D_6^+$ and its dehydrogenation products and Al_n^+ products with $n = 99, 98, 97$, etc. The kinetic energy thresholds for Al_{99}^+ , Al_{98}^+ , Al_{97}^+ , Al_{96}^+ , Al_{95}^+ , and Al_{94}^+ are all similar. If these products resulted from sequential loss of aluminum atoms by collision-induced dissociation

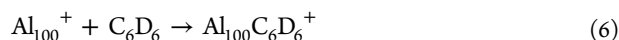


the thresholds would be expected to be shifted to significantly higher kinetic energies as the size of the product ion decreased. The fact that the thresholds are not shifted in this way suggests that the Al_n^+ products result from a chemical reaction such as



It is possible to write a whole series of plausible reactions that involve breaking up the C_6D_6 molecule. However, we did not have the ability to probe the composition of the neutral products in our experiments, so it was not possible to identify them. There have been a number of studies of the AlC_6H_6 complex.^{28,35–39} Theoretical and infrared resonance-enhanced multiphoton photodissociation (IR-REMPD) spectroscopy studies determined the dissociation energy of $\text{Al}^+(\text{C}_6\text{H}_6)$ to be 35.2 and 30.2 kcal/mol respectively.^{37,38} Silva and Head found the most stable complex to be a bridging structure with the aluminum atom bonded to two distinct carbon atoms across the ring.²⁸ Electron spin resonance (ESR) and IR-REMPD studies support a 6-fold axis of rotation with the metal atom above the ring.^{36,38} One could imagine a similar bonding scheme with aluminum atoms above and below the ring. However, no information seems to be available about the interaction between small aluminum clusters (i.e., Al_2 , Al_3 , Al_4 , and so on) and benzene.

The $\text{Al}_{100}\text{C}_6\text{D}_6^+$ product results from chemisorption of C_6D_6 onto the Al_{100}^+ cluster according to the reaction



The C_6D_6 molecule must be chemisorbed because $\text{Al}_{100}\text{C}_6\text{D}_6^+$ with a physisorbed C_6D_6 would not survive long enough to be detected at the elevated cluster temperatures employed here. Our experimental results provide no information about the structure of the $\text{Al}_{100}\text{C}_6\text{D}_6^+$ product, so we cannot determine whether the C_6D_6 is intact or dissociated on the Al_{100}^+ cluster.

Using angle-resolved ultraviolet photoelectron spectroscopy (ARUPS), high-resolution electron energy loss spectroscopy (HREELS), thermal desorption spectroscopy (TDS), work function measurements, and density functional theory (DFT), Duschek and co-workers concluded that the bonding between benzene and an sp-metal surface is distinctly different from that between benzene and a transition-metal surface.⁴ In both cases, the plane of the benzene molecule is oriented parallel with the surface. However, the bonding on transition metals involves charge transfer from the benzene π orbitals to the d bands of the metal and back-bonding into the π^* orbital of the molecule, resulting in substantial stabilization of the π orbitals.^{2,4} On $\text{Al}(111)$, a weakly bound state in which benzene is approximately 0.37 nm from the surface has been observed.⁴ HREELS confirmed C_{6v} symmetry for the benzene molecule on the surface, which is the same symmetry as for a free benzene molecule. If the molecule were strongly bonded to the $\text{Al}(111)$ surface, C_{3v} symmetry would be expected, as a result of the interactions between the benzene molecule and the surface.^{4,29} The weakly bound state described above cannot be responsible for the $\text{Al}_{100}\text{C}_6\text{D}_6^+$ adduct observed in our experiments. At the high temperatures used here, the benzene must be chemisorbed to the Al_{100}^+ cluster for the adduct to survive long enough to be detected.

Effect of Temperature on the Reaction Thresholds.

Below the Al_{100}^+ melting temperature (573 K), the cross sections for the Al_{99}^+ product increase rapidly for collision energies above 8 eV. Above the melting temperature (873 and

1073 K), the rapid increase starts at a significantly lower kinetic energy, closer to 7 than to 8 eV. This drop in the kinetic energy threshold is probably due to the melting transition. The threshold is lower for the liquid cluster than for the solid. However, this is not the whole story, because the cross sections for Al_{99}^+ (and the smaller Al_n^+ products) do not drop to zero at low collision energies. This suggests that another reaction pathway (with a much lower kinetic energy threshold) opens up to form these products on the liquid clusters.

Structural flexibility is often used to rationalize the reactivity of supported metal catalysts. However, it is unclear whether the results presented here provide insight into the behavior of oxide-supported metal nanoparticles. Support–catalyst interactions are known to play an important role in the reactivity of supported nanoparticles.^{10,40–45} Also, the structure of the Al_{100}^+ nanocluster is unknown; therefore, the characteristics of its surface, such as its facets, edges, and defects, are also unknown. Information about the surface is crucial for understanding catalytic activity.^{41–45}

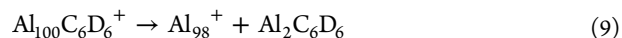
The behavior of the $\text{Al}_{100}\text{C}_6\text{D}_x^+$ products is also complex. At 573 K, the $\text{Al}_{100}\text{C}_6\text{D}_x^+$ products show a kinetic energy threshold of around 3–4 eV. Above the melting temperature, the threshold disappears, and the cross sections gradually increase and then decrease with increasing kinetic energy. In the measurements performed as a function of temperature with a fixed collision energy, the cross sections for the $\text{Al}_{100}\text{C}_6\text{D}_x^+$ products increase with increasing temperature, peak at around 650 K, and then start to decrease. The decrease starts to occur just after the cluster melts (639 K), suggesting that the phase transition is responsible. It is evident from Figure 6 that the dehydrogenation of $\text{Al}_{100}\text{C}_6\text{H}_6^+$ starts at around the same temperature. However, the decrease in the $\text{Al}_{100}\text{C}_6\text{D}_x^+$ cross sections is not due to dehydrogenation because the dehydrogenation products are included in the $\text{Al}_{100}\text{C}_6\text{D}_x^+$ cross sections. The decrease in the $\text{Al}_{100}\text{C}_6\text{D}_x^+$ cross sections could be due to loss of C_6D_6 from the $\text{Al}_{100}\text{C}_6\text{D}_6^+$ complex



Another plausible explanation for the decrease is that the $\text{Al}_{100}\text{C}_6\text{D}_6^+$ complex undergoes a chemical reaction in which the cluster breaks up, such as

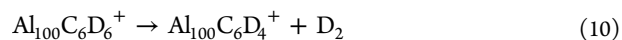


or

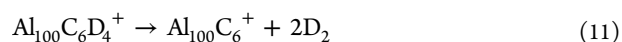


In Figure 4, the drop in the $\text{Al}_{100}\text{C}_6\text{D}_x^+$ cross sections that turns on at around 650 K is correlated with an increase in the cross sections for Al_{99}^+ and Al_{98}^+ .

Dehydrogenation. Below 600 K, the $\text{Al}_{100}\text{C}_6\text{D}_x^+$ product is entirely $\text{Al}_{100}\text{C}_6\text{D}_6^+$. Dehydrogenation begins at around 650 K (see Figure 6). Between 600 and 900 K, the first step in the dehydrogenation process, namely



dominates, and the amounts of $\text{Al}_{100}\text{C}_6\text{D}_2^+$ and $\text{Al}_{100}\text{C}_6^+$ are both small. Above 900 K the amount of $\text{Al}_{100}\text{C}_6^+$ increases steadily, whereas the amount of $\text{Al}_{100}\text{C}_6\text{D}_2^+$ remains small. This suggests that the losses of the second and third D_2 molecules are correlated



The mechanism by which a D₂ molecule is removed from chemisorbed C₆D₆ and released is not yet known. Perhaps the benzene begins to bury itself within the metallic cluster as the cluster melts. Marin et al. performed a DFT analysis of benzene dehydrogenation on Pt(111).⁵ Through an endothermic process, the authors proposed plausible pathways for the dehydrogenation of benzene on the platinum surface.⁵ The lowest-energy pathway first requires parallel binding of the benzene ring flat to the surface.⁵ This is followed by tilting of the ring such that two adjacent carbon atoms are bonded to the surface for the release of H₂.⁵

AUTHOR INFORMATION

Corresponding Author

*E-mail: mfj@indiana.edu.

Notes

The authors declare no competing financial interest.

ACKNOWLEDGMENTS

We gratefully acknowledge the support of the National Science Foundation through Grant 0911462.

REFERENCES

- (1) Waddill, G. D.; Kesmodel, L. L. Benzene Chemisorption on Palladium Surfaces. I. High-Resolution Electron-Energy-Loss Vibrational Spectra and Structural Models. *Phys. Rev. B: Condens. Matter* **1985**, *31*, 4940–4946.
- (2) Jing, Z. The Adsorption of Benzene on Ni(111). *Surf. Sci.* **1991**, *250*, 147–158.
- (3) Günster, J.; Liu, G.; Kempter, V.; Goodman, D. W. Adsorption of Benzene on Mo(100) and MgO(100)/Mo(100) Studied by Ultraviolet Photoelectron and Metastable Impact Electron Spectroscopies. *Surf. Sci.* **1998**, *415*, 303–311.
- (4) Duschek, R.; Mittendorfer, F.; Blyth, R. I. R.; Netzer, F. P.; Hafner, J.; Ramsey, M. G. The Adsorption of Aromatics on sp-Metals: Benzene on Al(111). *Chem. Phys. Lett.* **2000**, *318*, 43–48.
- (5) Saeys, M.; Reyniers, M.-F.; Neurock, M.; Marin, G. Density Functional Theory Analysis of Benzene (De)hydrogenation on Pt(111): Addition and Removal of the First Two H-Atoms. *J. Phys. Chem. B* **2003**, *107*, 3844–3855.
- (6) Caputo, R.; Prascher, B.; Staemmler, V.; Bagus, P.; Woll, C. Adsorption of Benzene on Coinage Metals: A Theoretical Analysis Using Wavefunction-Based Methods. *J. Phys. Chem.* **2007**, *111*, 12778–12784.
- (7) Freund, H. J.; Messmer, R. P. On the Bonding and Reactivity of CO₂ on Metal Surfaces. *Surf. Sci.* **1986**, *172*, 1–30.
- (8) Onishi, H.; Aruga, T.; Iwasawa, Y. Switchover of Reaction Paths in the Catalytic Decomposition of Formic Acid on TiO₂(110) Surface. *J. Catal.* **1994**, *146*, 557–567.
- (9) Freund, H. J.; Roberts, M. W. Surface Chemistry of Carbon Dioxide. *Surf. Sci. Rep.* **1996**, *25*, 225–273.
- (10) Ngo, L.; Xu, L.; Grant, A.; Campbell, C. Benzene Adsorption and Dehydrogenation on Pt/ZnO(0001)-O Model Catalysts. *J. Phys. Chem. B* **2003**, *107*, 1174–1179.
- (11) Pawlow, P. Über die Abhängigkeit des Schmelzpunktes von der Oberflächenenergie eines Festen Körpers. *Z. Phys. Chem.* **1909**, *65*, 1–35.
- (12) Takagi, M. Electron-Diffraction Study of Liquid-Solid Transition of Thin Metal Films. *J. Phys. Soc. Jpn.* **1954**, *9*, 359–363.
- (13) Peppiatt, S. A. The Melting of Small Particles. I. Lead. *Proc. R. Soc. London, Ser. A* **1975**, 401–412.
- (14) Buffat, P.; Borell, J. P. Size Effect on the Melting Temperature of Gold Particles. *Phys. Rev. A: At. Mol. Opt. Phys.* **1976**, *13*, 2287–2298.
- (15) Schmidt, M.; Kusche, R.; Kronmüller, W.; von Issendorff, B.; Haberland, H. Experimental Determination of the Melting Point and

Heat Capacity for a Free Cluster of 139 Sodium Atoms. *Phys. Rev. Lett.* **1997**, *79*, 99–102.

(16) Schmidt, M.; Kusche, R.; von Issendorff, B.; Haberland, H. Irregular Variations in the Melting Point of Size-Selected Atomic Clusters. *Nature* **1998**, *393*, 238–240.

(17) Schmidt, M.; Haberland, H. Phase Transitions in Clusters. *C. R. Phys.* **2002**, *3*, 327–340.

(18) Haberland, H.; Hippler, T.; Donges, J.; Kostko, O.; Schmidt, M.; von Issendorff, B. Melting of Sodium Clusters: Where Do the Magic Numbers Come from? *Phys. Rev. Lett.* **2005**, *94*, 035701.

(19) Neal, C. M.; Starace, A. K.; Jarrold, M. F. Ion Calorimetry: Using Mass Spectrometry to Measure Melting Points. *J. Am. Soc. Mass Spectrom.* **2007**, *18*, 74–81.

(20) Chirot, F.; Feiden, P.; Zamith, S.; Labastie, P.; L'Hermite, J. M. A Novel Experimental Method for the Measurement of the Caloric Curves of Clusters. *J. Chem. Phys.* **2008**, *129*, 164514.

(21) Aguado, A.; Jarrold, M. F. Melting and Freezing of Metal Clusters. *Annu. Rev. Phys. Chem.* **2001**, *62*, 151–172.

(22) Breaux, G.; Hillman, D.; Neal, C.; Benirschke, R.; Jarrold, M. F. Gallium Cluster “Magic Melters”. *J. Am. Chem. Soc.* **2004**, *126*, 8628–8629.

(23) Neal, C. M.; Starace, A. K.; Jarrold, M. F.; K., J.; Krishnamurthy, S.; Kanhere, D. G. Melting of Aluminum Cluster Cations with 31–48 Atoms: Experiment and Theory. *J. Phys. Chem.* **2007**, *111*, 17788–17794.

(24) Starace, A. K.; Cao, B.; Judd, O. H.; Bhattacharyya, I.; Jarrold, M. F. Melting of Size-Selected Aluminum Nanoclusters with 84–128 Atoms. *J. Chem. Phys.* **2010**, *132*, 034302.

(25) Cao, B.; Starace, A. K.; Judd, O. H.; Jarrold, M. F. Melting Dramatically Enhances the Reactivity of Aluminum Nanoclusters. *J. Am. Chem. Soc.* **2009**, *131*, 2446–2447.

(26) Leslie, K. L.; Shinholt, D.; Jarrold, M. F. Reactions of CO₂ on Solid and Liquid Al₁₀₀⁺. *J. Phys. Chem. A* **2012**, ASAP.

(27) Cao, B.; Starace, A. K.; Judd, O. H.; Bhattacharyya, I.; Jarrold, M. F.; Lopez, J. M.; Aguado, A. Activation of Dinitrogen by Solid and Liquid Aluminum Nanoclusters. A Combined Experimental and Theoretical Study. *J. Am. Chem. Soc.* **2010**, *132*, 12906–12918.

(28) Silva, S. J.; Head, J. D. A Theoretical Investigation of the Aluminum–Benzene Complex. *J. Am. Chem. Soc.* **1992**, *114*, 6479–6484.

(29) Moskovits, M.; DiLella, D. P. Surface-Enhanced Raman Spectroscopy of Benzene and Benzene-*d*₆ Adsorbed on Silver. *J. Chem. Phys.* **1980**, *73*, 6068–6075.

(30) Garfunkel, E. L.; Minot, C.; Gavezzotti, A.; Simonetta, M. Benzene Adsorption on the Rh(111) Metal Surface: A Theoretical Study. *Surf. Sci.* **1986**, 177–197.

(31) Sun, Y.; Khang, S. Catalytic Membrane for Simultaneous Chemical Reaction and Separation Applied to a Dehydrogenation Reaction. *Ind. Eng. Chem. Res.* **1988**, *27*, 1136–1142.

(32) Zakin, M. R.; Cox, D. M.; Kaldor, A. Reaction of Niobium Clusters with Benzene-*h*₆ and -*d*₆: Evidence for Cluster-Induced Dehydrogenation. *J. Phys. Chem.* **1987**, *91*, S224–S228.

(33) St. Pierre, R.; Chronister, E.; El-Sayed, M. Photochemical Dehydrogenation of Benzene Chemisorbed on Small Niobium Metal Clusters. *J. Phys. Chem.* **1987**, *91*, S228–S234.

(34) Neal, C. M.; Breaux, G. A.; Cao, B.; Starace, A. K.; Jarrold, M. F. Improved Signal Stability From a Laser Vaporization Source with a Liquid Metal Target. *Rev. Sci. Instrum.* **2007**, *78*, 075108.

(35) Mighell, A. D.; Himes, V. L.; Hubbard, C. R. Aluminum Atom–Benzene Molecular Complex: Matrix Isolation Electron Spin Resonance Study. *J. Am. Chem. Soc.* **1979**, *101*, 5860–5862.

(36) Howard, J. A.; Joly, H. A.; Mile, B. Electron Spin Resonance Spectra and Structure of Al(C₆H₆) in Hydrocarbon Matrices. *J. Am. Chem. Soc.* **1989**, *111*, 8094–8098.

(37) Stöckigt, D. Cation- π Interaction in Al(L)⁺ Complexes (L = C₆H₆, C₅H₅N, C₅H₆, C₄H₄NH, C₄H₄O). *J. Phys. Chem. A* **1997**, *101*, 3800–3807.

(38) van Heijnsbergen, D.; Jaeger, T. D.; von Helden, G.; Meijer, G.; Duncan, M. A. The Infrared Spectrum of Al^+ -Benzene in the Gas Phase. *Chem. Phys. Lett.* **2002**, *364*, 345–351.

(39) Miyajima, K.; Yabushita, S.; Knickelbein, M. B.; Nakajima, A. Stern–Gerlach Experiments of One-Dimensional Metal–Benzene Sandwich Clusters: $\text{M}_n(\text{C}_6\text{H}_6)_m$ ($\text{M} = \text{Al}, \text{Sc}, \text{Ti}, \text{and V}$). *J. Am. Chem. Soc.* **2007**, *129*, 8473–8480.

(40) Davis, S. M.; Somorjai, G. A. In *The Chemical Physics of Solid Surfaces and Heterogeneous Catalysis*; King, D. A., Woodruff, D. P., Eds.; Elsevier: Amsterdam, 1982; Vol. 4, pp 217–298.

(41) Clair, T. P. S.; Goodman, D. W. Metal Nanoclusters Supported on Metal Oxide Thin Films: Bridging the Materials Gap. *Top. Catal.* **2000**, *13*, 5–19.

(42) Henry, C. R. Catalytic Activity of Supported Nanometer-Sized Metal Clusters. *Appl. Surf. Sci.* **2000**, *164*, 252–259.

(43) Zheng, N.; Stucky, G. D. A General Synthetic Strategy for Oxide-Supported Metal Nanoparticle Catalysts. *J. Am. Chem. Soc.* **2006**, *128*, 14278–14280.

(44) Mathew, S.; Kumara, C. S.; Nagaraju, N. Influence of Nature of Support on the Catalytic Activity of Supported Molybdenum-Oxo Species in Benzyl Alcohol Conversion. *J. Mol. Catal. A: Chem.* **2006**, *255*, 243–248.

(45) Castleman, A. W., Jr. Cluster Structure and Reactions: Gaining Insights into Catalytic Processes. *Catal. Lett.* **2001**, *141*, 1243–1253.